Supporting information

Selective, sensitive and reversible "turn-on" fluorescent cyanide probes based on 2,2'-dipyridylaminoanthracene-Cu^{2+} ensembles

Yongshu Xie,*[a] Yubin Ding,[a] Xin Li,[a] Cheng Wang,[a] Jonathan P. Hill,*[b] Katsuhiko Ariga,[b] Weibing Zhang,[a] and Weihong Zhu[a]

[a]*Key Laboratory for Advanced Materials and Institute of Fine Chemicals, East China University of Science and Technology, Shanghai, P. R. China.; E-mail: yshxie@ecust.edu.cn; Fax: (+86) 21-6425-2758. Tel: (+86) 21-6425-0772.*

[b]*WPI-Center for Materials Nanoarchitectonics, National Institute for Materials Science (NIMS), Namiki 1-1, Tsukuba, Ibaraki, Japan.*

Contents:

Fig. S19. Job's plot for determining the stoichiometry of **2** and Cu^{2+}.

Fig. S20. Plot of ΔF_{438nm} vs. $[Cu^{2+}]$ for **1**. λ_{ex} = 360 nm. The best fit line to the equation, superimposed on the data, yields K_{ass} of 6×10^5 M^{-1}.

Fig. S21. Plot of ΔF_{437nm} vs. $[Cu^{2+}]$ for **2**. λ_{ex} = 298 nm. The best fit line to the equation, superimposed on the data, yields K_{ass} of 1.0×10^5 M^{-1}.

Fig. S22. a) Fluorescence changes during the titration of **1** (10 μM) with Cu^{2+} (0-4 equiv.), b) Plot of $(I_{max} - I)/(I_{max}-I_{min})$ vs $Log([Cu^{2+}])$, the calculated detection limit of **1** for Cu^{2+} is 3×10^{-7} M.

Fig. S23. a) Fluorescence changes during the titration of **2** (10 μM) with Cu^{2+} (0-2 equiv.), b) Plot of $(I_{max} - I)/(I_{max}-I_{min})$ vs $Log([Cu^{2+}])$, the calculated detection limit of **2** for Cu^{2+} is 9×10^{-7} M.

Fig. S24. a). UV-Vis spectral changes during titration of **3** (10 μM) with Cu^{2+} (0-210 equiv.) in MeOH/H_2O, 4/1, v/v. b). Corresponding fluorescence emission spectral changes with λ_{ex} fixed at 375 nm (one of the isosbestic points).

Fig. S25. Plot of ΔF_{437nm} vs. $[Cu^{2+}]$ for **3**. λ_{ex} = 375 nm. The best fit line to the equation, superimposed on the data, yields K_{ass} of 2.2×10^3 M^{-1}.

Fig. S26. Complementary views of the crystal structure of compound **3** with ellipsoids shown at the 20% probability level.

Fig. S27. Optimized molecular structure of compound **1**.

Fig. S28. Optimized molecular structure of compound **2**.

Fig. S29. Optimized molecular structure of compound **3**.

Fig. S30. UV-Vis spectral changes during titration of **1-Cu^{2+}** (10 μM) with CN^- in MeOH/H_2O (4/1, v/v)

Fig. S31. Fluorescence emission spectral changes during the titration of **1-Cu^{2+}** (10 μM) with CN^- in MeOH/H_2O (4/1, v/v), with λ_{ex} fixed at 360 nm.

Fig. S32. Fluorescence emission spectral changes during titration of **2-Cu^{2+}** (10 μM) with CN^- in MeOH/H_2O (4/1, v/v), with λ_{ex} fixed at 298 nm.

Fig. S33. Plots of ^{1}H NMR spectra of **1** (20 mM) on successive addition of Cu^{2+} and CN^- in DMSO-d_6.

Fig. S34. Plots of ^{1}H NMR spectra of **2** (20 mM) on successive addition of Cu^{2+} and CN^- in DMSO-d_6.

Fig. S35. Fluorescence emission spectral changes during titration of **3-Cu^{2+}** (10 μM) with CN^- (0-90 equiv.) in MeOH/H_2O (4/1, v/v), with λ_{ex} fixed at 375 nm.

Fig. S36. a) Fluorescence changes during the titration of **1** (2 μM) **- Cu^{2+}** (4.0 eq) with CN^- (0-2.0 equiv.), b) Plot of $(I-I_{min})/(I_{max}-I_{min})$ vs $Log([CN^-])$, the calculated detection limit of **1-Cu^{2+}** is 3×10^{-7} M.

Fig. S37. a) Fluorescence changes during the titration of **2** (0.5 μM) **- Cu^{2+}** (2.75 eq) with CN^- (0-3.6 equiv.), b) Plot of $(I-I_{min})/(I_{max}-I_{min})$ vs $Log([CN^-])$, the calculated detection limit of **2-Cu^{2+}** is 2×10^{-7} M.

Fig. S38. a) Changes in the emission spectrum of **2-Cu^{2+}** (10 μM) in the presence of various anions (20 equiv. for CN^-, 100 equiv. for F^-, Cl^-, Br^-, I^-, AcO^-, $H_2PO_4^-$, CO_3^{2-}, SO_4^{2-}, SCN^-, S^{2-}) in MeOH/H_2O, 4/1, v/v; b) White bars represent the addition of 100 eq. of various anions (for CN^-: 20 eq.). Black bars represent the addition of 100 equiv. of indicated anions, followed by 20 equiv. of CN^- anions. 1~12: no anions, CN^-, F^-, Cl^-, Br^-, I^-, AcO^-, $H_2PO_4^-$, CO_3^{2-}, SO_4^{2-}, SCN^-, and S^{2-}.

Fig. S39. Emission intensity changes of **2-Cu^{2+}** with alternately added CN^- and Cu^{2+}.

Fig. S40. Time course of the fluorescence response of **1** (10 μM) and **1-Cu^{2+}** (10 μM) in MeOH/H_2O, 4:1, v:v (λ_{ex} = 360 nm, λ_{em} = 438 nm): a) Compound **1** upon addition of 4 equiv. of Cu^{2+}; b) **1- Cu^{2+}** upon addition of 12 equiv. of CN^-.

Fig. S41. Time course of the fluorescence response of **2** (10 μM) and **2-Cu^{2+}** (10 μM) in MeOH/H_2O, 4:1, v:v (λ_{ex} = 298 nm, λ_{em} = 437 nm): a) Compound **2** upon addition of 2 equiv. of Cu^{2+}; b) **2- Cu^{2+}** upon addition of 8 equiv. of CN^-.

Fig. S42. Fluorescence emission of **1** (10 μM, black squares), **1**+4 eq Cu^{2+} (red circles), and **1**+4 eq Cu^{2+}+ 12 eq CN^- (green triangles) over the pH range 5-12.

Fig. S43. Fluorescence emission of **2** (10 μM, black squares), **2**+2 eq Cu^{2+} (red circles), and **2**+2 eq Cu^{2+}+ 8 eq CN^- (green triangles) over the pH range 5-12.

Experimental section

Apparatus and Instruments

UV-Vis absorption spectra were recorded on a Varian Cary 100 spectrophotometer and fluorescence spectra were recorded on a Varian Cary Eclipse fluorescence spectrophotometer, with sample solutions in a quartz cuvette (path length = 1 cm). All fluorescence spectra are uncorrected. ^{1}H NMR and ^{13}C NMR spectra were obtained using a Bruker AVANCE spectrometer (400 MHz). High resolution mass spectra were measured on a Waters LCT Premier XE spectrometer.

Reagents and General procedures

Dichloromethane was distilled from CaH_2, and THF was distilled from sodium using benzophenone ketyl as the indicator. Unless specified otherwise all other solvents were used as commercially supplied. Deuterated solvents for NMR measurements were obtained from Aldrich. All syntheses were performed in Schlenk tubes under N_2, and monitored by using thin-layer chromatography. Column chromatography was carried out in air using silica gel (200-300 mesh). Compounds 1a[1], 2a[2] and 3a[3] were synthesized according to literature methods.

Fluorescence emission spectral measurements

The fluorescence emission spectral changes of **1**~**3** and **1-Cu^{2+}**~**3-Cu^{2+}** during the titrations were measured at 25 °C in MeOH/H_2O (4:1), with excitation wavelength set at one of the corresponding isosbestic points. The slit width was 5 nm and PMT voltage was 510 V for both excitation and emission. Tested ions Cu^{2+}, Zn^{2+}, Cd^{2+}, Hg^{2+}, Ni^{2+}, Mn^{2+}, and Ca^{2+} were added as perchlorate salts dissolved in MeOH. Anions such as F^-, Cl^-, Br^-, I^-, AcO^-, $H_2PO_4^-$ were added as TBA salts dissolved in MeOH, other anions as CO_3^{2-}, SO_4^{2-}, SCN^- and S^{2-} were added as sodium salts. Fluorescence changes were measured immediately after addition of cations or anions, because the interaction processes between **1**~**2** with Cu^{2+} or **1-Cu^{2+}**~**2-Cu^{2+}** with CN^- are very fast (Fig. S40, S41).

Quantum yield measurements

The luminescence quantum yields in solution were measured using anthracene ($\Phi_{standard}$ = 0.28 in EtOH[4]) as a reference. The quantum yield Φ_{sample} as a function of solvent polarity was calculated using the following equation[5]:

$$\Phi_{sample} = \Phi_{standard} \times \left(\frac{F_{sample}}{F_{standard}}\right) \times \left(\frac{Abs_{standard}}{Abs_{sample}}\right) \times \left(\frac{n_{sample}}{n_{standard}}\right)^2$$

where Φ is the quantum yield, Abs is the absorbance of the solution, F is the corrected emission

intensity and n is the average refractive index of the solution. Subscripts standard and sample refer to the reference and unknown compound, respectively.

Crystallography

Single crystals suitable for X-ray analysis of **3** were obtained by slow evaporation of a chloroform-hexane solution at room temperature.

Crystal data for **3**: $C_{24}H_{17}N_3$, Mw = 347.41 g·mol^{-1}, 0.25 × 0.19 × 0.17 mm^3, orthorhombic, P212121, a = 8.6890(12), b = 11.6597(16), c = 16.959(2) Å, V = 1718.1(4) Å^3, F(000) = 728, ρ_{calcd} = 1.343 Mg·m^{-3}, μ(Mo-Kα) = 0.080 mm^{-1}, T = 293(2) K, 12909 data were measured on a Bruker SMART Apex diffractometer, of which 3013 were unique (R_{int} = 0.0377); 245 parameters were refined against Fo^2 (all data), final wR_2 = 0.0954, S = 1.130, R_1 ($I > 2\sigma(I)$) = 0.0404, largest final difference peak/hole = +0.171/-0.184 eÅ^{-3}. The structure was solved by direct methods and refined with full matrix least-squares technique against F^2 (all data) using SHELXTL.

Detection Limits

The detection limits of probes **1** and **2** for Cu^{2+} and **1-Cu^{2+}** and **2-Cu^{2+}** for CN^- were obtained according to the literature method.[6] Take **1-Cu^{2+}** for CN^- as the example: Compound **1** (2 μM) was dissolved in a mixture of MeOH/H_2O (4/1), Cu^{2+} was added to quench its fluorescence, forming an ensemble of **1-Cu^{2+}**. Fluorescence changes during the titration of **1-Cu^{2+}** with CN^- (0-4 μM) in MeOH/H_2O (4/1) is shown in Figure S36a. The enhancement of fluorescence intensity is clearly resolved with a good signal to noise ratio. The inset of Figure S36a shows the plot of $(I-I_{min})/(I_{max}-I_{min})$ versus log[CN^-]. Where I_{max} represents the maximum fluorescence intensity when 2 equiv. of cyanide was added, and I_{min} represents the minimum fluorescence intensity of **1-Cu^{2+}** ensemble before the addition of cyanide. Four intermediate values were selected for linear regression as shown in Figure S36b. The intercept of the line at the x-axis was taken as the detection limit. Thus, the detection limit of **1-Cu^{2+}** for CN^- was calculated to be 3 × 10^{-7} M.

Determination of the Association Constants

The association constants can be calculated from the fluorescence intensity changes at a fixed wavelength. In the case of a 1:1 stoichiometry, the following equation[7] can be used for the nonlinear fitting to calculate the association constant:

$$F = \frac{b}{2C_L K_{ass}} (K_{ass}C_M + C_L K_{ass} + 1 - \sqrt{(K_{ass}C_M + C_L K_{ass} + 1)^2 - 4C_L C_M K_{ass}^2})$$

Where C_L is the concentration of the ligand, K_{ass} is the association constant, C_M is the concentration of the metal ions, F is the corresponding fluorescence intensity, and b is a fitting parameter. So K_{ass} can thus be obtained by a nonlinear least-squares fitting of F versus C_M.

DFT calculations of the molecular structures of 1~3

The optimized structures of compounds **1~3** in MeOH (Figs. S27~ S29) were calculated by using the Gaussian03 program package.[8] The geometries of all compounds were optimized by density functional calculations employing the hybrid B3LYP function and 6-31G* basis set.[9] Molecular structures and molecular orbitals were visualized by the Gabedit software.[10].

Synthesis of compound **1b**:

A mixture of Et_2NH (5 mL), **1a** (500 mg, 2 mmol), $Pd(PPh_3)_2Cl_2$ (28 mg, 0.04 mmol), and CuI (5 mg, 0.03 mmol) was degassed and flushed with nitrogen. Then, trimethylsilylacetylene (490 mg, 5 mmol) was injected. The mixture was stirred at 40°C for 2.5 h, and then quenched with water (25 ml). The product was extracted with dichloromethane (3 × 10 mL), dried over anhydrous Na_2SO_4 and solvents evaporated under reduced pressure. The residue was purified by column chromatography to afford *N*-(pyridin-2-yl)-6-[(trimethylsilyl)ethynyl]pyridin-2-amine as the intermediate. This was dissolved in THF (25 mL) then a THF (25 mL) solution of n-Bu_4NF (1.3 g, 5 mmol) was added at room temperature. The reaction mixture was stirred for 4 h. After removal of the solvent, the residue was subjected to column chromatography to give **1b** as a yellowish solid (195 mg, 50% yield (two steps)). ^{1}H NMR (d^6-DMSO, Bruker 400 MHz, 298K): δ = 9.86 (s, 1H, NH), 8.22 (d, 1H, J = 4 Hz, pyridyl), 7.85 (d, 1H, J = 8.4 Hz, pyridyl), 7.70-7.62 (m, 3H, pyridyl), 7.05 (d, 1H, J = 7.2 Hz, pyridyl), 6.89 (t, 1H, J = 5.8 Hz, pyridyl), 4.23 (s, 1H, alkynyl) ppm. ^{13}C NMR (d_6-DMSO, Bruker 100 MHz, 298K): δ = 154.28, 154.07, 147.32, 139.16, 137.98, 137.61, 119.46, 116.14, 112.19, 111.82, 83.26, 79.07 ppm. HRMS: obsd 196.0876, calcd for $C_{12}H_{10}N_3$ ($[M+H]^+$): 196.0875.

Synthesis of compound **1**:

1b (600 mg, 3.07mmol), 9-bromoanthracene (1.34 g, 5.22 mmol), $Pd(PPh_3)_2Cl_2$ (216 mg, 0.05 mmol), CuI (10 mg, 0.031 mmol), and $^iPr_2NH$ (12 mL) were added to THF (50 ml), and the mixture was stirred at 70°C for 15 h. After cooling to room temperature, the reaction mixture was quenched with water and the product was extracted with dichloromethane (3 × 100 mL), dried over anhydrous Na_2SO_4 and the solvents evaporated under reduced pressure. The crude material was purified by column chromatography to give **1** as a yellow solid (500 mg, 40% yield). ^{1}H NMR (d^6-DMSO, Bruker 400 MHz): δ = 10.00 (s, 1H, NH), 8.77 (s, 1H, anthryl), 8.61 (d, 2H, J = 8.4 Hz, anthryl), 8.28 (d, 1H, J = 4.4 Hz, pyridyl), 8.21 (d, 2H, J = 8.4 Hz, anthryl), 8.06 (d, 1H, J = 8.4 Hz, pyridyl), 7.84-7.63 (m, 7H, pyridyl and anthryl), 7.46 (d, 1H, J = 7.2 Hz, pyridyl), 6.93 (t, 1H, J = 6.4 Hz, pyridyl) ppm. ^{13}C NMR (d_6-DMSO, Bruker 100 MHz, 298K): δ = 154.52, 154.28, 147.30, 139.97, 138.17, 137.63, 132.16, 130.68, 129.03, 128.83, 127.67, 126.12, 125.73, 119.76, 116.13, 115.02, 112.13, 112.02, 100.65, 83.94 ppm. HRMS: obsd 372.1498, calcd for $C_{26}H_{18}N_3$ ($[M+H]^+$): 372.1501.

Synthesis of compound **2b**:

A mixture of Et_2NH (5 mL), **2a** (500 mg, 1.52 mmol), $Pd(PPh_3)_2Cl_2$ (28 mg, 0.04 mmol), and CuI (5 mg, 0.03 mmol) was degassed and flushed with nitrogen. Then trimethylsilylacetylene (600 mg, 6.12 mmol) was injected, and the mixture was stirred at 40°C for 2.5 h. The reaction mixture was quenched with water and the product was extracted with dichloromethane (3 × 10 mL), dried over anhydrous Na_2SO_4 then the solvents evaporated under reduced. The residue was purified by column chromatography to give bis{6-[(trimethylsilyl)ethynyl]pyridin-2-yl}-amine as an intermediate. This was dissolved in THF (30 mL), then a THF (30 mL) solution of n-Bu_4NF (1.56 g, 6 mmol) was added at room temperature. The reaction mixture was stirred for 4 h. After removal of the solvent, the residue was subjected to column chromatography to give **2b** as yellowish solid (161 mg, 48% yield over two steps). ^{1}H NMR (d_6-DMSO, Bruker 400 MHz): δ = 10.1 (s, 1H, NH), 7.76-7.69 (m, 4H, pyridyl),7.08 (d, 2H, J = 8Hz),4.27 (s, 2H, alkynyl) ppm. ^{13}C

NMR (d_6-DMSO, Bruker 100 MHz, 298K): δ = 159.25, 144.38, 143.45, 125.08, 117.55, 88.43, 84.54 ppm. HRMS: obsd 220.0873, calcd for $C_{14}H_{10}N_3$ ([M+H]$^+$): 220.0875.

Synthesis of compound **2**:

A mixture of **2b** (300 mg, 1.37 mmol), 9-bromoanthracene (846 mg, 3.28 mmol), $Pd(PPh_3)_4$ (168 mg, 0.144 mmol), CuI (30 mg, 0.09 mmol), $^iPr_2NH$ (18 mL) and THF (30 mL) was degassed and flushed with nitrogen, and the mixture was stirred at 70°C for 21 h. After cooling, the reaction mixture was quenched with water and the product was extracted with dichloromethane, dried over anhydrous Na_2SO_4 and evaporated in vacuo. The residue was purified by column chromatography to give **2** as a yellow solid (270 mg, 30% yield). ^{1}H NMR (d^6-DMSO, Bruker 400 MHz): δ = 10.33 (s, 1H, NH), 8.79 (s, 2H, anthryl), 8.64 (d, 4H, J = 8.4 Hz, anthryl), 8.23 (d, 4H, J = 8.4 Hz, anthryl), 8.03 (d, 2H, J = 8.4 Hz, anthryl), 7.92 (t, 2H, J = 5.8 Hz, pyridyl), 7.79 (t, 4H, J = 7.4 Hz, anthryl), 7.67 (t, 4H, J = 7.4 Hz, anthryl), 7.53 (d, 2H, J = 3.6 Hz, pyridyl) ppm. HRMS: obsd 572.2125, calcd for $C_{42}H_{26}N_3$ ([M+H]$^+$): 572.2127.

Synthesis of compound **3**:

2,2'-Dipyridylamine (1.23 g, 7.0 mmol), 9-bromoanthracene (0.77 g, 3.0 mmol), anhydrous potassium carbonate (1.66 g, 12.0 mmol), cupric sulfate (91 mg, 0.63 mmol), and diphenyl ether (2 mL) were added to a Schlenk tube, degassed, flushed with N_2 and then heated at 200°C for 3 days. After the reaction had cooled, dichloromethane and water were added to dissolve the solid, and the organic phase was washed with water to neutral pH and then dried with Na_2SO_4. After removal of the solvent, the residue was purified by a silica gel column to afford compound **3** (322 mg, 31% yield). ^{1}H NMR (d_6-DMSO, Bruker 400 MHz): δ = 8.74 (s, 1H, anthryl-meso-H), 8.20 (d, 2H, J = 8.8 Hz, anthryl), 8.13 (q, 2H), 7.92 (d, 2H, J = 8.4 Hz, anthryl), 7.63-7.58 (m, 2H), 7.54-7.50 (m, 2H), 7.47-7.43 (m, 2H), 7.00 (d, 2H, J = 8.4 Hz, anthryl), 6.95-6.92 (m, 2H) ppm. HRMS: obsd 348.1422, calcd for $C_{24}H_{18}N_3$ ([M+H]$^+$): 348.1501.

References

[1] M. h. Yang, C. C. Chou, H. C. Lee, G. H. Lee, M. k. Leung and S. M. Peng, *Chemical Communications* **1997**, 2279-2280.

[2] E. X. Zhang, D. X. Wang, Z. T. Huang and M. X. Wang, *The Journal of Organic Chemistry* **2009**, *74*, 8595-8603.

[3] a) D. Maiti, B. P. Fors, J. L. Henderson, Y. Nakamura and S. L. Buchwald, *Chemical Science* **2011**, *2*, 57-68; b) C. Tu, J. Lin, Y. Shao and Z. Guo, *Inorganic Chemistry* **2003**, *42*, 5795-5797.

[4] a) C. A. Parker. and W. T. Rees., *Analyst* **1960**, *85*, 587-600; b) D. F. Eaton, *Pure & Appl. Chem* **1988**, *60*, 1107-1114.

[5] A. T. R. Williams, S. A. Winfield and J. N. Miller, *Analyst* **1983**, *108*, 1067-1071

[6] M. Shortreed, R. Kopelman, M. Kuhn and B. Hoyland, *Anal. Chem*., 1996, 68, 1414-1418.

[7] J. Bourson, J. Pouget and B. Valeur, *J. Phys. Chem.* 1993, **97**, 4552-4557.

[8] Gaussian 03, Revision D.01, M. J. Frisch, G. W. Trucks, H. B. Schlegel, G. E. Scuseria, M. A. Robb, J. R. Cheeseman, J. A. Montgomery, Jr., T. Vreven, K. N. Kudin, J. C. Burant, J. M. Millam, S. S. Iyengar, J. Tomasi, V. Barone, B. Mennucci, M. Cossi, G. Scalmani, N. Rega, G. A. Petersson, H. Nakatsuji, M. Hada, M. Ehara, K. Toyota, R. Fukuda, J. Hasegawa, M. Ishida, T. Nakajima, Y. Honda, O. Kitao, H. Nakai, M. Klene, X. Li, J. E. Knox, H. P. Hratchian, J. B. Cross, V. Bakken, C. Adamo, J. Jaramillo, R. Gomperts, R. E. Stratmann, O. Yazyev, A. J. Austin, R. Cammi, C. Pomelli, J. W. Ochterski, P. Y. Ayala, K. Morokuma, G. A. Voth, P. Salvador, J. J. Dannenberg, V. G. Zakrzewski, S. Dapprich, A. D. Daniels, M. C. Strain, O. Farkas, D. K. Malick, A. D. Rabuck, K. Raghavachari, J. B. Foresman, J. V. Ortiz, Q. Cui, A. G. Baboul, S. Clifford, J. Cioslowski, B. B. Stefanov, G. Liu, A. Liashenko, P. Piskorz, I. Komaromi, R. L. Martin, D. J. Fox, T. Keith,

M. A. Al-Laham, C. Y. Peng, A. Nanayakkara, M. Challacombe, P. M. W. Gill, B. Johnson, W. Chen, M. W. Wong, C. Gonzalez, and J. A. Pople, Gaussian, Inc., Wallingford CT, 2004.

[9] (a) A. D. Becke, J. Chem. Phys., 1993, 98, 5648; (b) C. Lee, W. Yang and R. G. Parr, *Phys. Rev. B*, 1988, **37**, 785.

[10] A.-R. Allouche, *J. Comput. Chem*., 2011, **32**, 174.

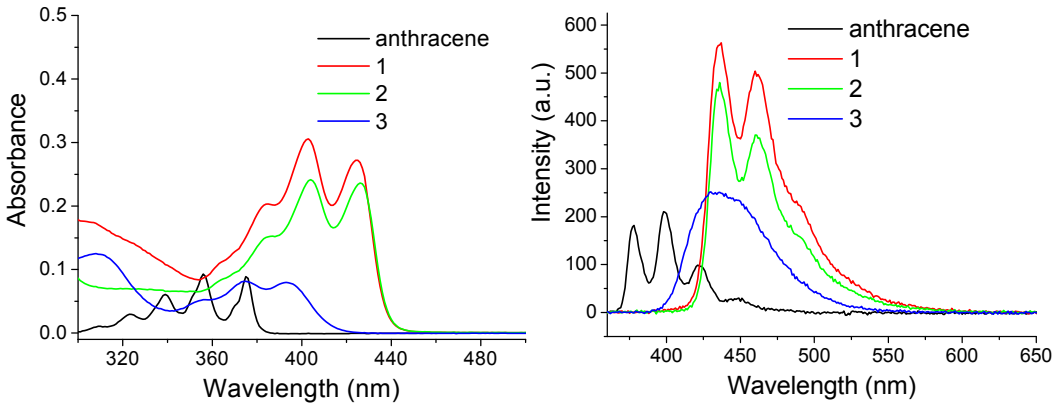

Fig. S1. Quantum yield (Φ_f) measurements: a) absorption spectra of anthracene and **1**–**3** (10 μM) in EtOH. b) Fluorescence spectra of anthracene and **1**–**3** (10 μM) in EtOH, with the excitation wavelength of 350 nm.

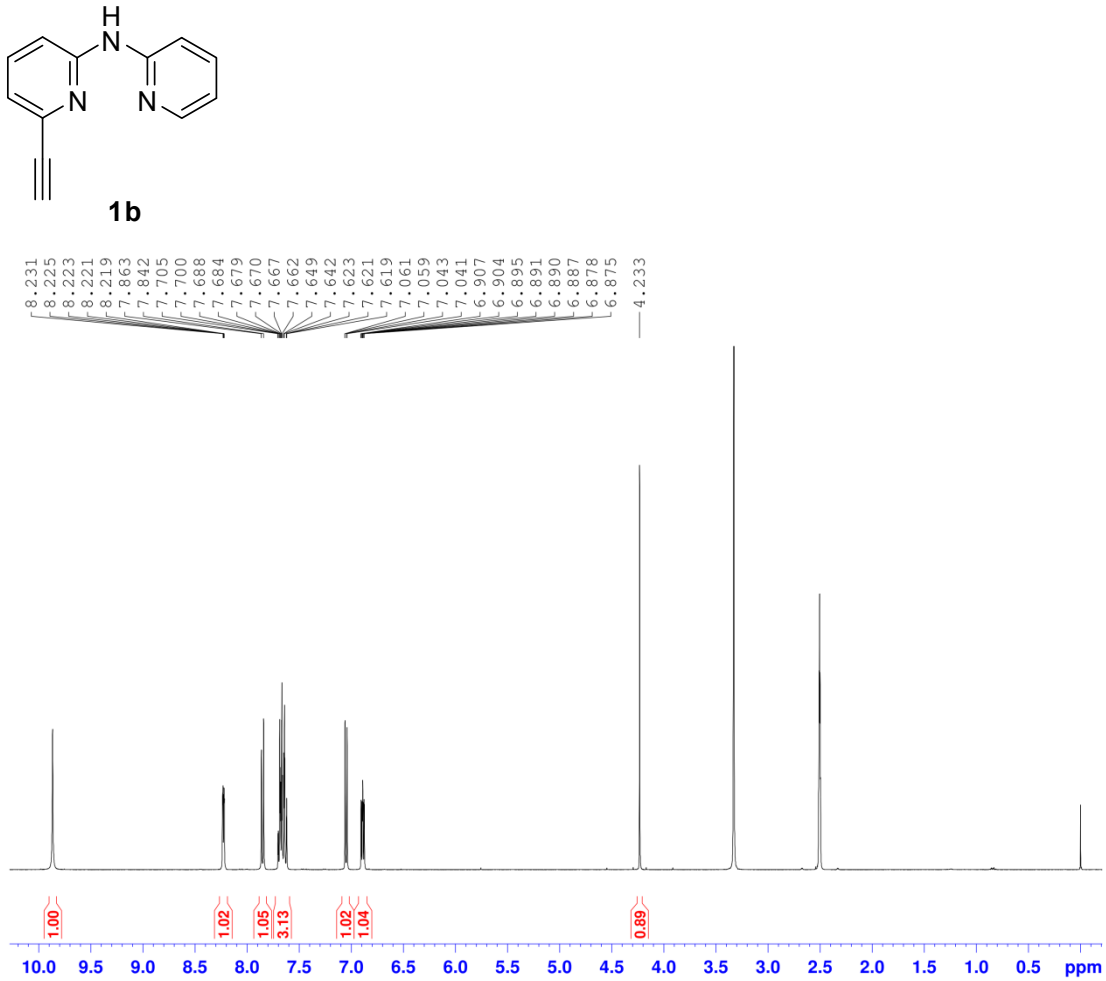

Fig. S2. ^{1}H NMR spectrum of **1b** in DMSO-d_6.

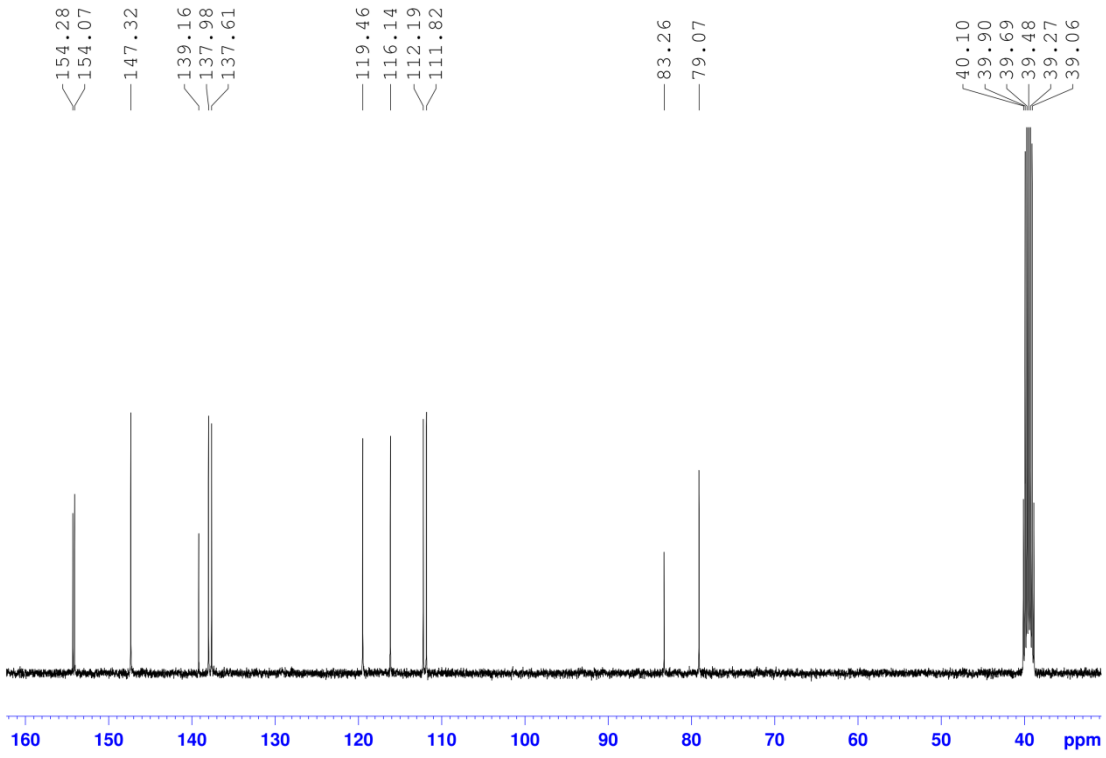

Fig. S3. ^{13}C NMR spectrum of **1b** in DMSO-d_6.

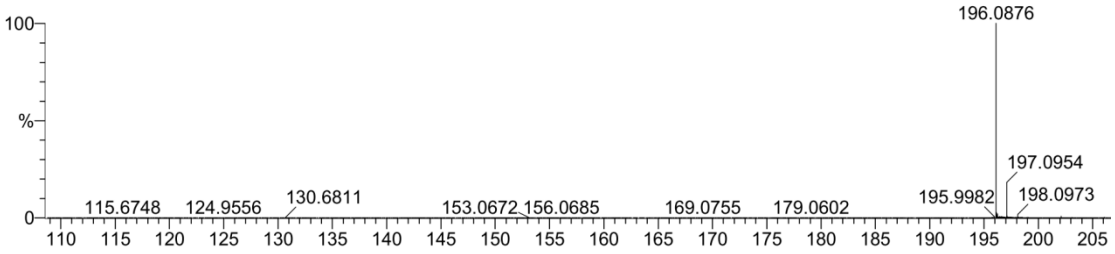

Fig. S4. HRMS of **1b** in MeOH.

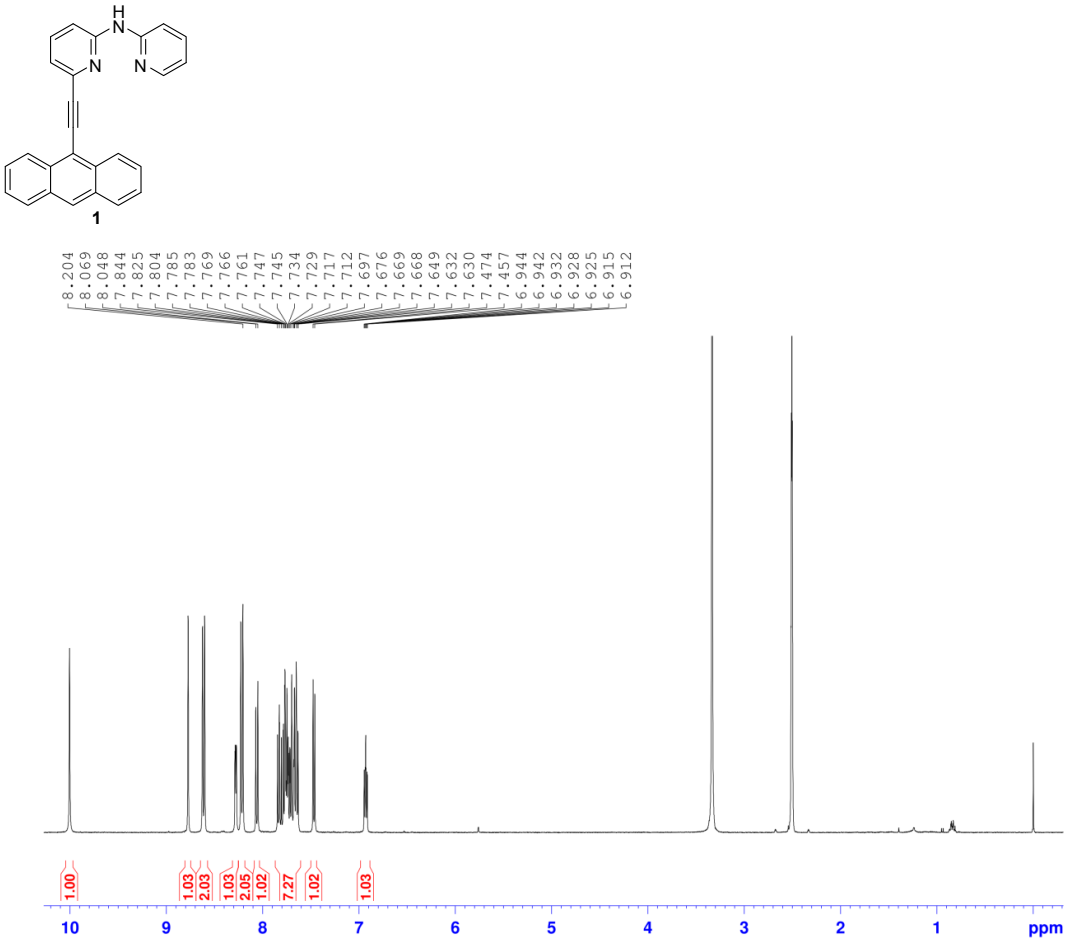

Fig. S5. ^{1}H NMR spectrum of **1** in DMSO-d_6.

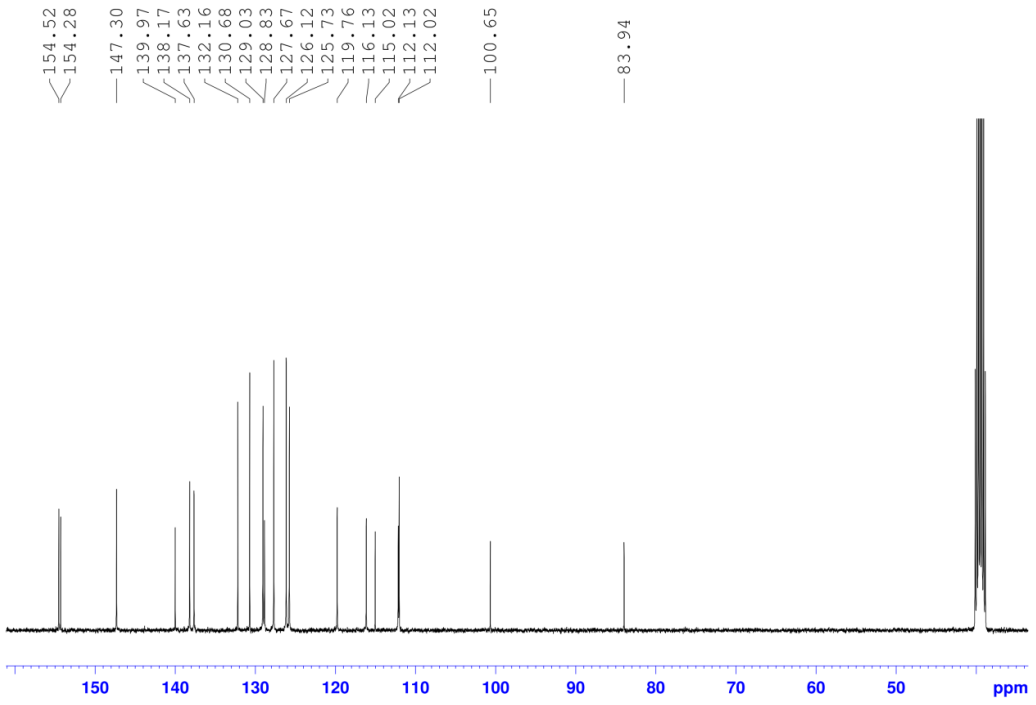

Fig. S6. ^{13}C NMR spectrum of **1** in DMSO-d_6.

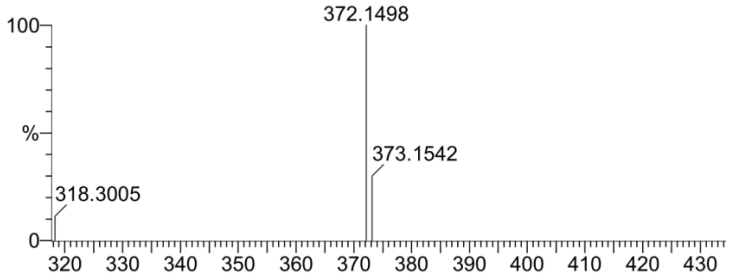

Fig. S7. HRMS of **1** in MeOH.

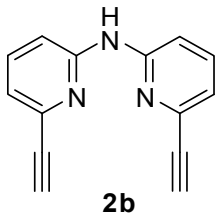

2b

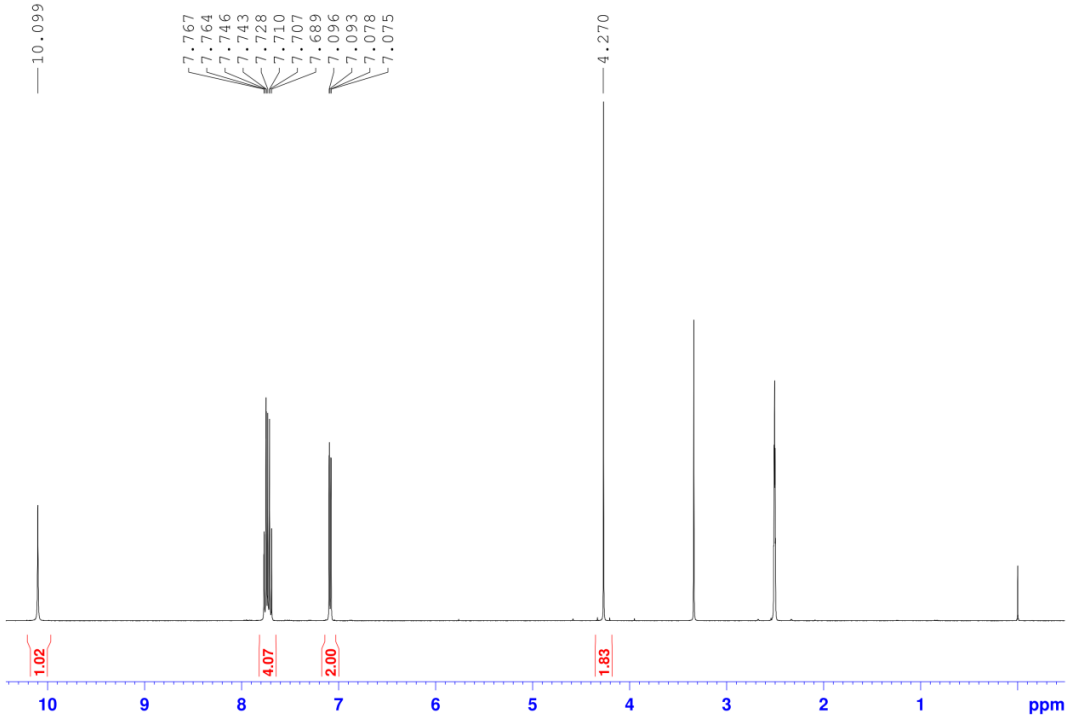

Fig. S8. ^{1}H NMR spectrum of **2b** in DMSO-d_6.

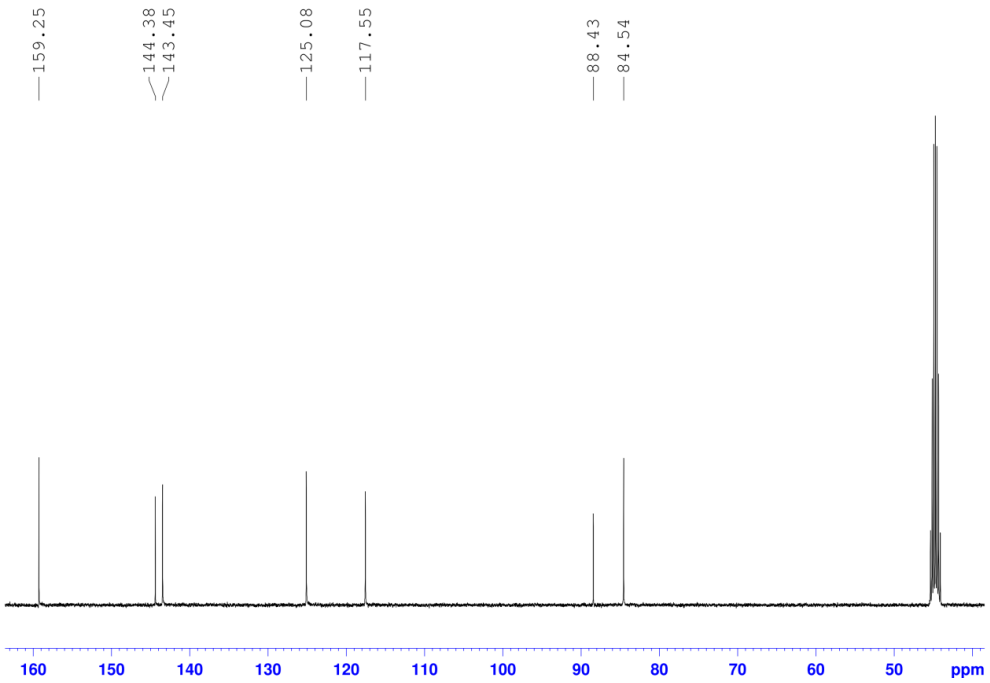

Fig. S9. ^{13}C NMR spectrum of **2b** in DMSO-d_6.

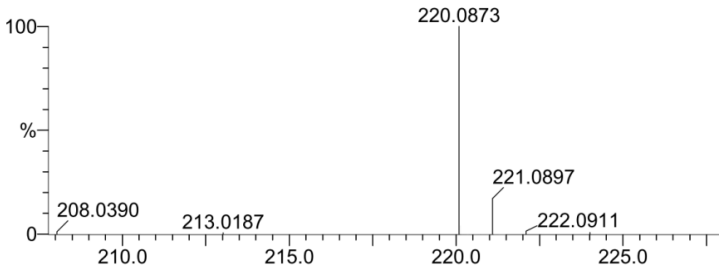

Fig. S10. HRMS of **2b** in MeOH.

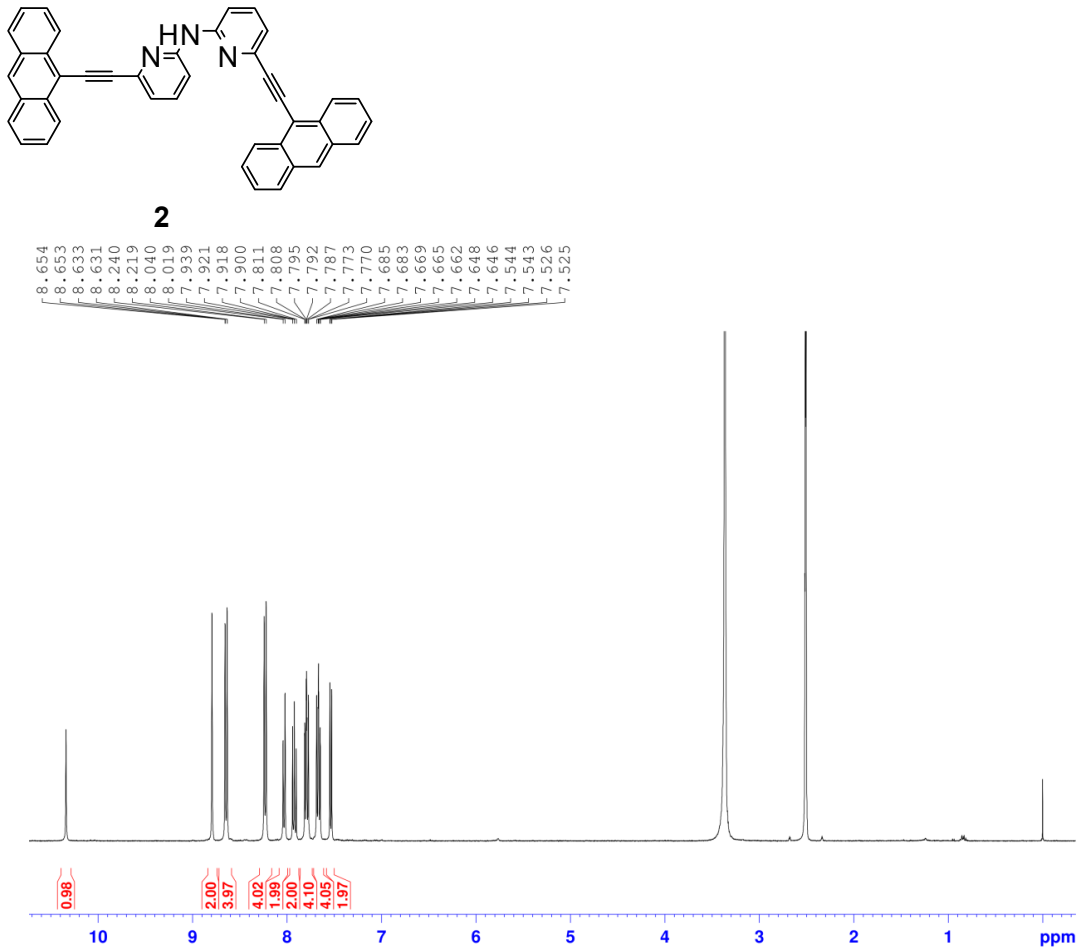

Fig. S11. ^{1}H NMR spectrum of **2** in DMSO-d_6.

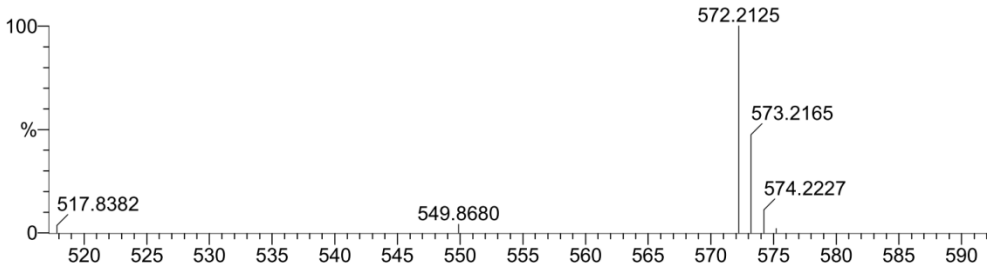

Fig. S12. HRMS of **2** in MeOH.

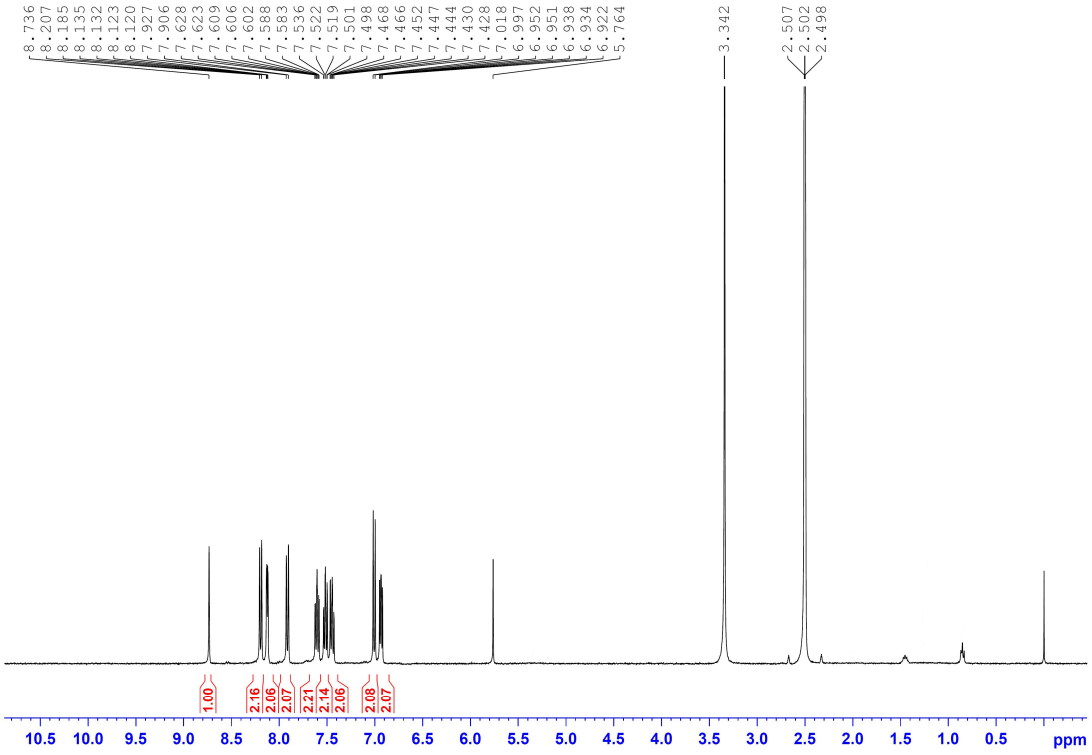

Fig. S13. ^{1}H NMR spectrum of **3** in DMSO-d_6.

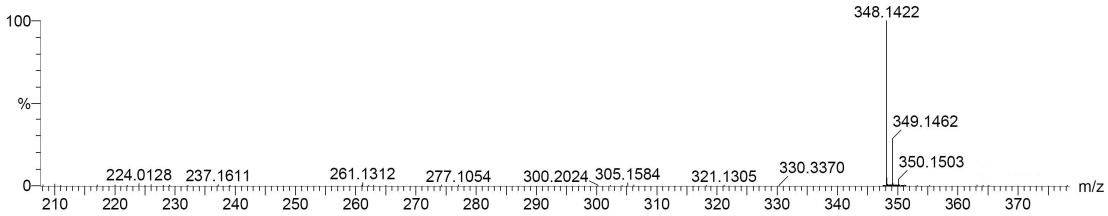

Fig. S14. HRMS of **3** in MeOH.

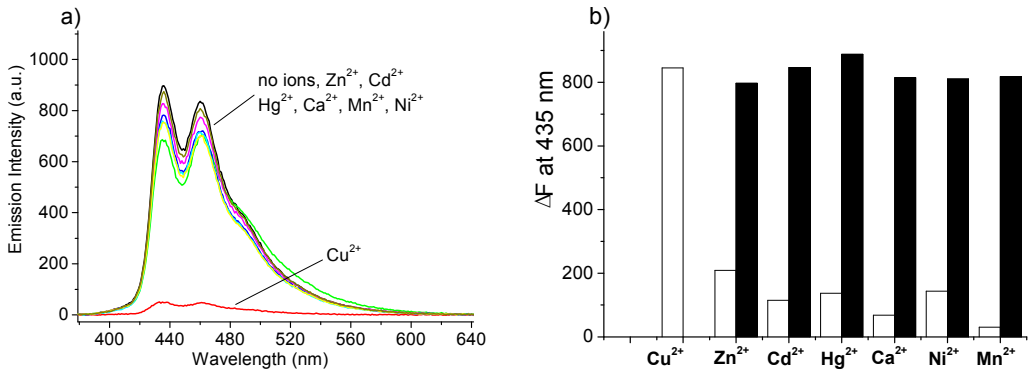

Fig. S15. a) Fluorescence spectra (λ_{ex} = 360 nm) of **1** (10 μM) in the presence of various metal ions in MeOH/H_2O, 4/1, v/v. b) White bars represent the addition of 50 equiv. of metal ions to a 10 μM solution of **1**, for Cu^{2+}: 5 eq. Black bars represent the addition of 5.0 equiv. of Cu^{2+} mixed with 50 equiv. of other metal ions to a 10 μM solution of **1**.

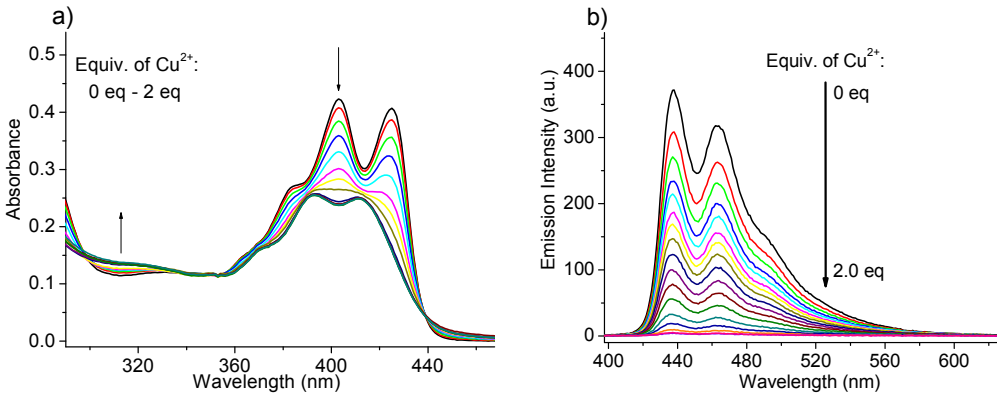

Fig. S16. a) UV-Vis spectral changes during titration of **2** (10 μM) with Cu^{2+} (0-2.0 equiv.) in MeOH/H_2O, 4/1, v/v. b). Corresponding fluorescence emission spectral changes with λ_{ex} fixed at 298 nm (one of the isosbestic points).

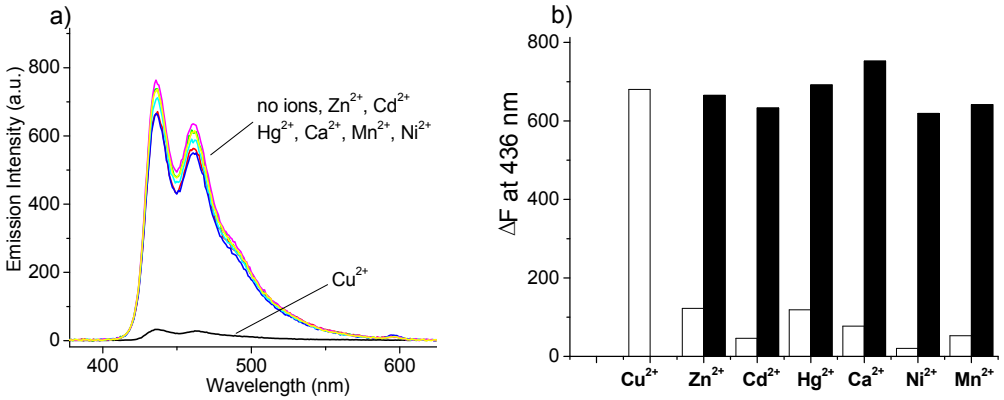

Fig. S17. a) Fluorescence spectra (λ_{ex} = 298 nm) of **2** (10 μM) in the presence of various metal ions in MeOH/H_2O, 4/1, v/v. b) White bars represent the addition of 50 equiv. of metal ions to a 10 μM solution of **2**, for Cu^{2+}: 5 eq. Black bars represent the addition of 5.0 equiv. of Cu^{2+} mixed with 50 equiv. of other metal ions to a 10 μM solution of **2**.

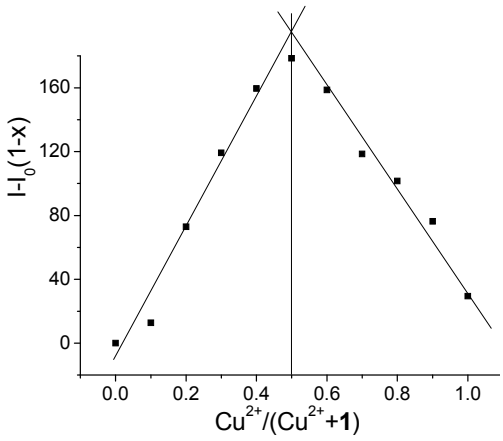

Fig. S18. Job's plot for determining the stoichiometry of **1** and Cu^{2+}.

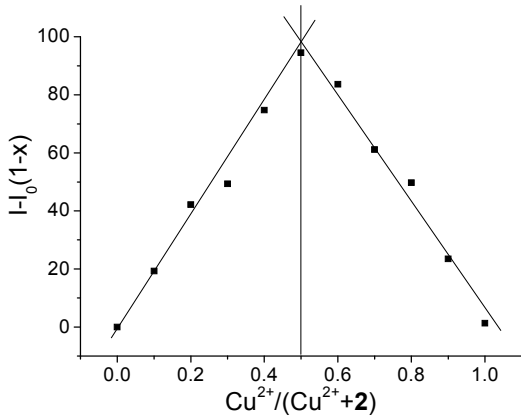

Fig. S19. Job's plot for determining the stoichiometry of **2** and Cu^{2+}.

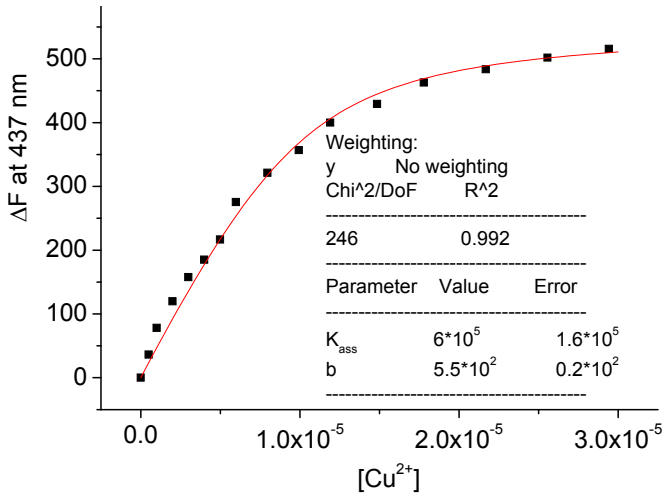

Fig. S20. Plot of ΔF_{438nm} vs. $[Cu^{2+}]$ for **1**. λ_{ex} = 360 nm. The best fit line to the equation, superimposed on the data, yields K_{ass} of 6×10^5 M^{-1}.

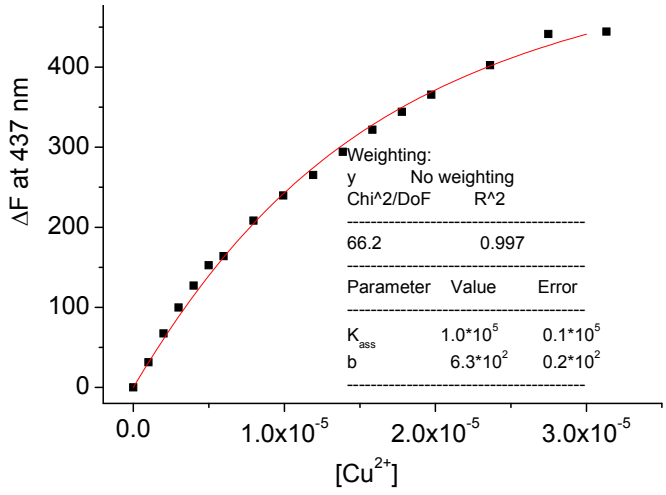

Fig. S21. Plot of ΔF_{437nm} vs. $[Cu^{2+}]$ for **2**. λ_{ex} = 298 nm. The best fit line to the equation, superimposed on the data, yields K_{ass} of 1.0×10^5 M^{-1}.

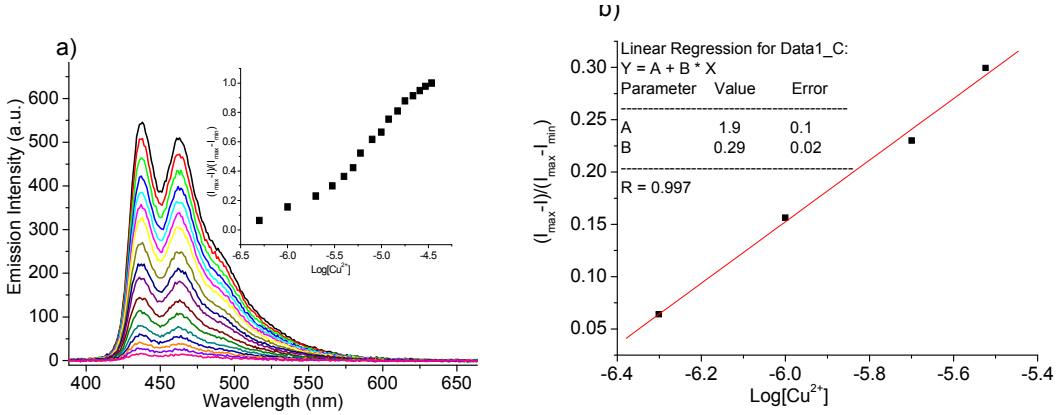

Fig. S22. a) Fluorescence changes during the titration of **1** (10 μM) with Cu^{2+} (0-4 equiv.), b) Plot of $(I_{max} - I)/(I_{max}-I_{min})$ vs Log($[Cu^{2+}]$), the calculated detection limit of **1** for Cu^{2+} is 3×10^{-7} M.

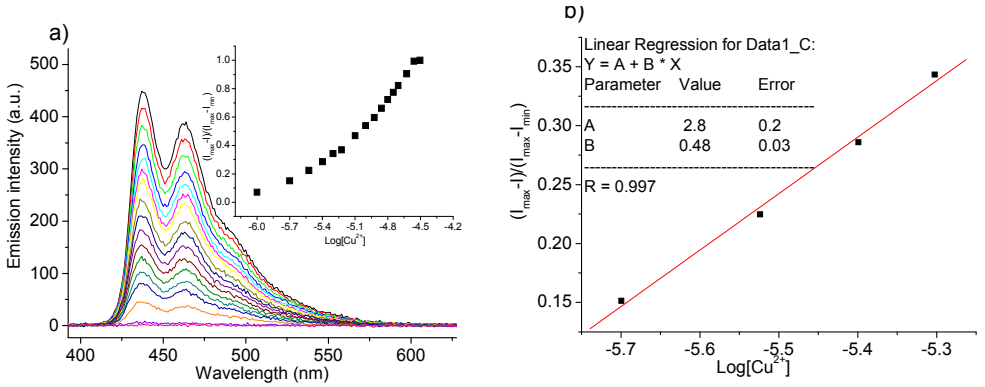

Fig. S23. a) Fluorescence changes during the titration of **2** (10 μM) with Cu^{2+} (0-2 equiv.), b) Plot of $(I_{max} - I)/(I_{max}-I_{min})$ vs Log($[Cu^{2+}]$), the calculated detection limit of **2** for Cu^{2+} is 9×10^{-7} M.

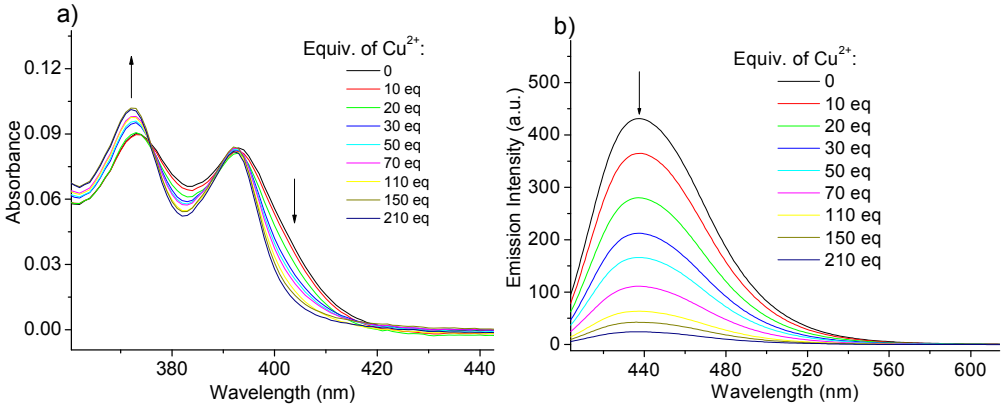

Fig. S24. a). UV-Vis spectral changes during titration of **3** (10 μM) with Cu^{2+} (0-210 equiv.) in MeOH/H_2O, 4/1, v/v. b). Corresponding fluorescence emission spectral changes with λ_{ex} fixed at 375 nm (one of the isosbestic points).

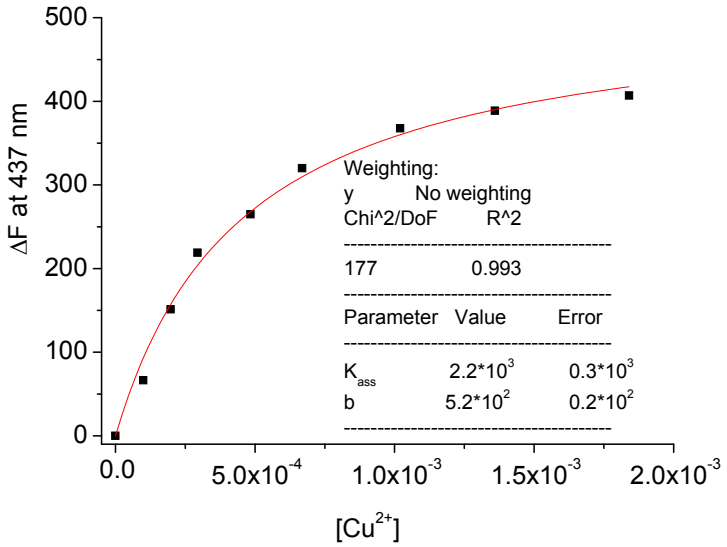

Fig. S25. Plot of ΔF_{437nm} vs. $[Cu^{2+}]$ for **3**. λ_{ex} = 375 nm. The best fit line to the equation, superimposed on the data, yields K_{ass} of 2.2×10^3 M^{-1}.

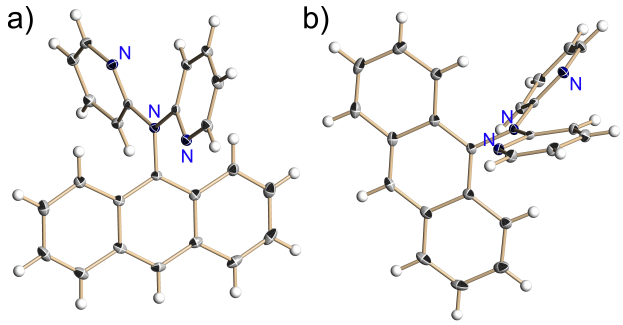

Fig. S26. Complementary views of the crystal structure of compound **3** with ellipsoids shown at the 20% probability level.

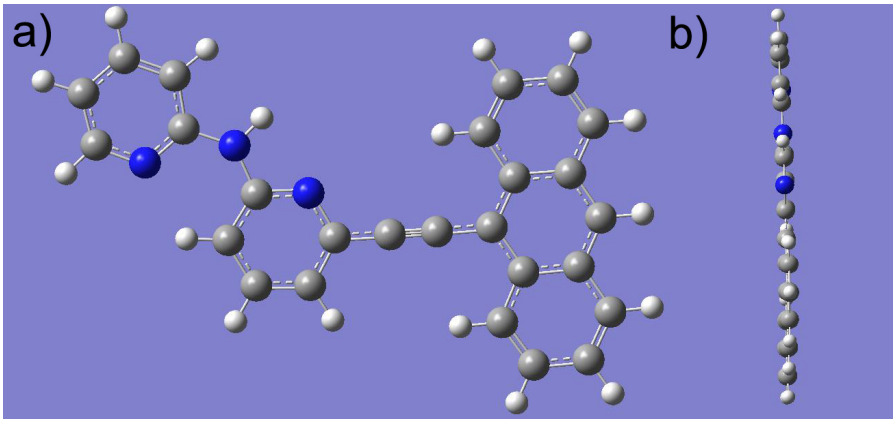

Fig. S27. Optimized molecular structure of compound **1**.

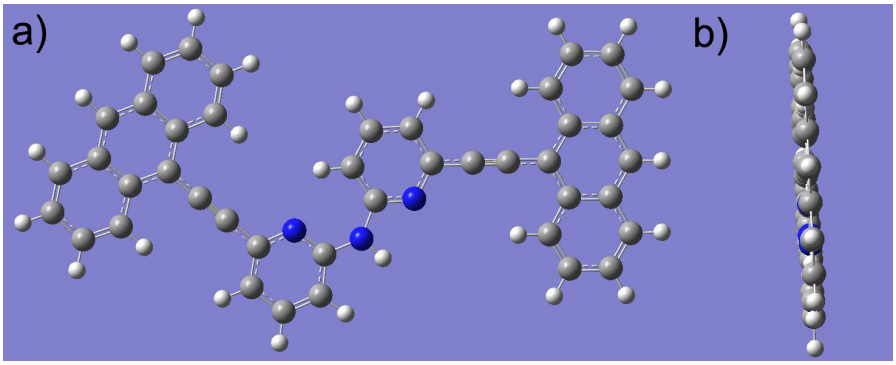

Fig. S28. Optimized molecular structure of compound **2**.

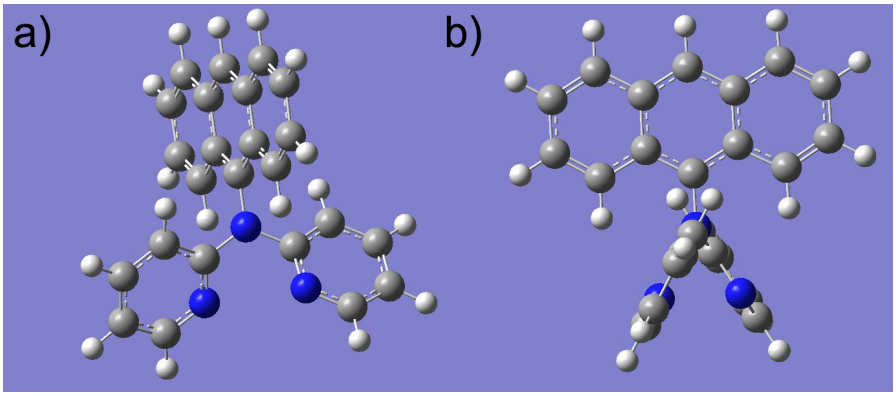

Fig. S29. Optimized molecular structure of compound **3**.

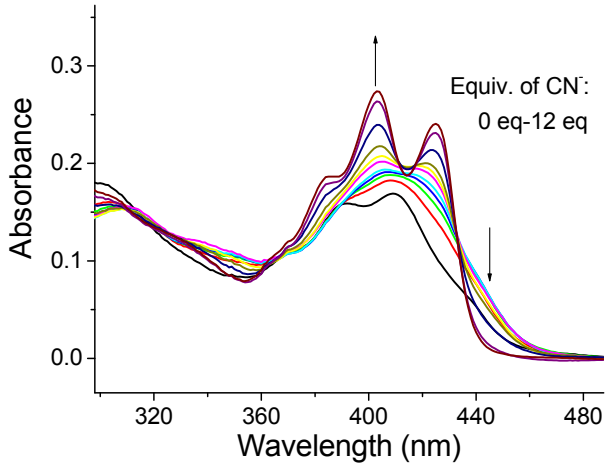

Fig. S30. UV-Vis spectral changes during titration of **1-Cu**$^{2+}$ (10 μM) with CN^- in MeOH/H_2O (4/1, v/v)

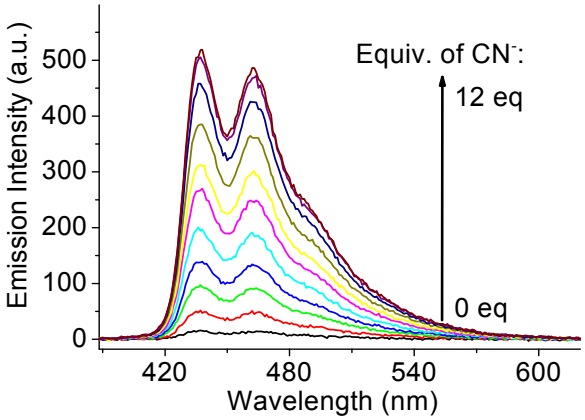

Fig. S31. Fluorescence emission spectral changes during the titration of **1-Cu**$^{2+}$ (10 μM) with CN^- in MeOH/H_2O (4/1, v/v), with λ_{ex} fixed at 360 nm.

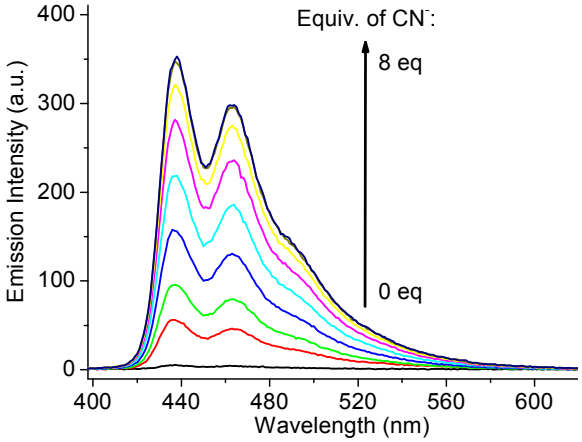

Fig. S32. Fluorescence emission spectral changes during titration of **2-Cu**$^{2+}$ (10 μM) with CN^- in MeOH/H_2O (4/1, v/v), with λ_{ex} fixed at 298 nm.

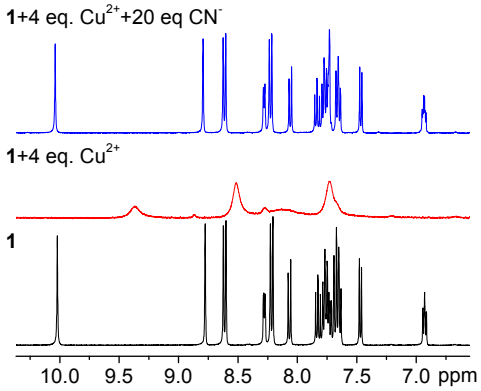

Fig. S33. Plots of ^1H NMR spectra of **1** (20 mM) on successive addition of Cu^{2+} and CN^- in DMSO-d_6.

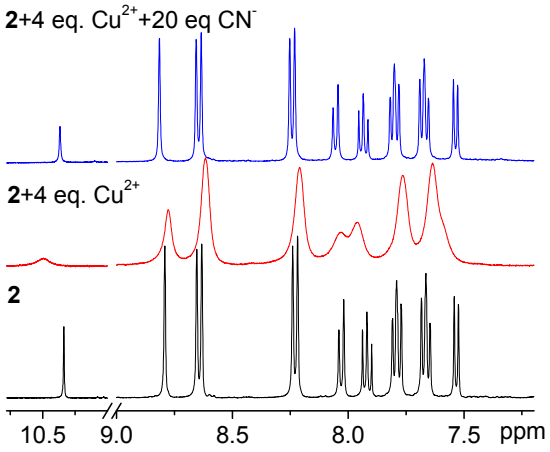

Fig. S34. Plots of ^{1}H NMR spectra of **2** (20 mM) on successive addition of Cu^{2+} and CN^- in DMSO-d_6.

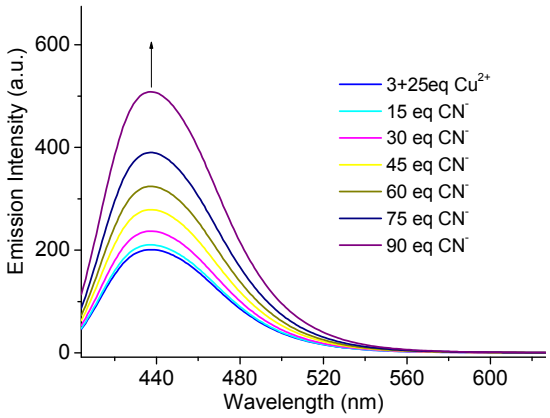

Fig. S35. Fluorescence emission spectral changes during titration of **3-Cu^{2+}** (10 μM) with CN^- (0-90 equiv.) in MeOH/H_2O (4/1, v/v), with λ_{ex} fixed at 375 nm.

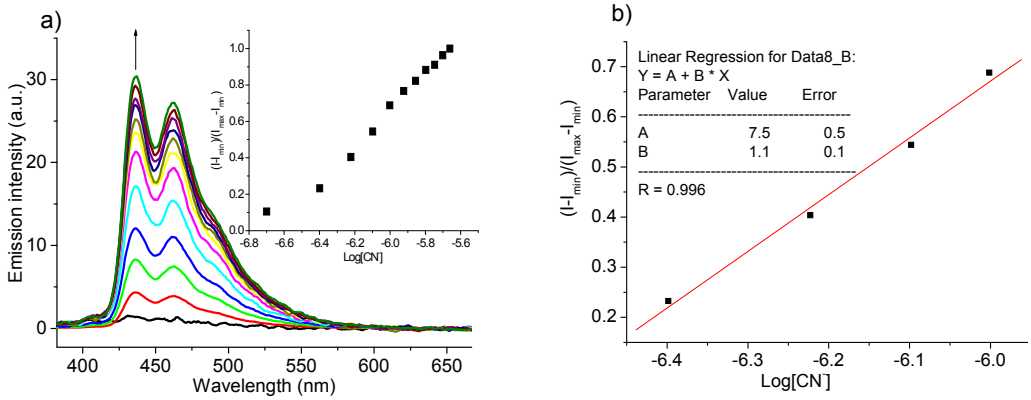

Fig. S36. a) Fluorescence changes during the titration of **1** (2 μM) - **Cu^{2+}** (4.0 eq) with CN^- (0-2.0 equiv.), b) Plot of $(I-I_{min})/(I_{max}-I_{min})$ vs Log($[CN^-]$), the calculated detection limit of **1-Cu^{2+}** is 3×10^{-7} M.

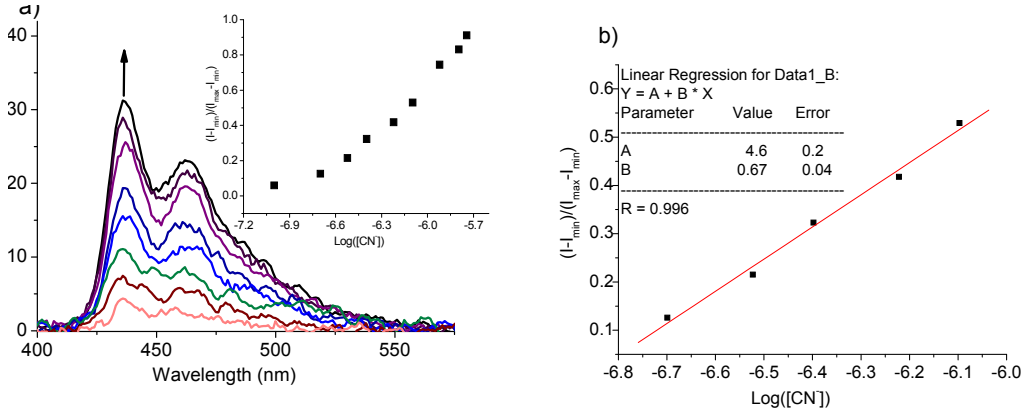

Fig. S37. a) Fluorescence changes during the titration of **2** (0.5 μM) - **Cu^{2+}** (2.75 eq) with CN^- (0-3.6 equiv.), b) Plot of $(I-I_{min})/(I_{max}-I_{min})$ vs Log([CN^-]), the calculated detection limit of **2-Cu^{2+}** is 2×10^{-7} M.

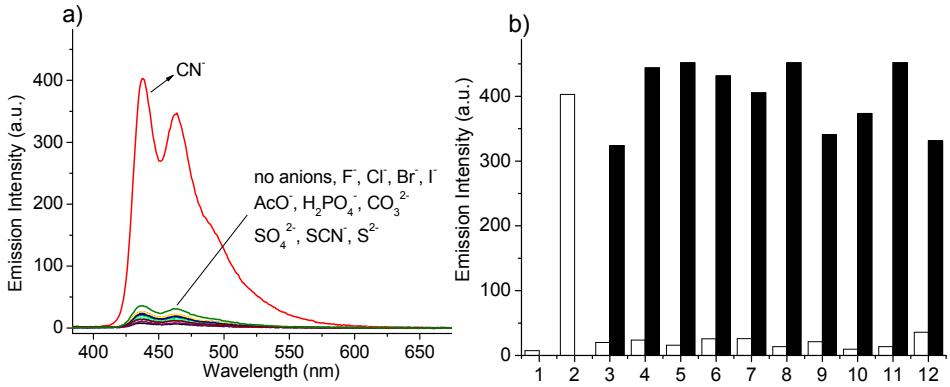

Fig. S38. a) Changes in the emission spectrum of **2-Cu^{2+}** (10 μM) in the presence of various anions (20 equiv. for CN^-, 100 equiv. for F^-, Cl^-, Br^-, I^-, AcO^-, $H_2PO_4^-$, CO_3^{2-}, SO_4^{2-}, SCN^-, S^{2-}) in MeOH/H_2O, 4/1, v/v; b) White bars represent the addition of 100 eq. of various anions (for CN^-: 20 eq.). Black bars represent the addition of 100 equiv. of indicated anions, followed by 20 equiv. of CN^- anions. 1~12: no anions, CN^-, F^-, Cl^-, Br^-, I^-, AcO^-, $H_2PO_4^-$, CO_3^{2-}, SO_4^{2-}, SCN^-, and S^{2-}.

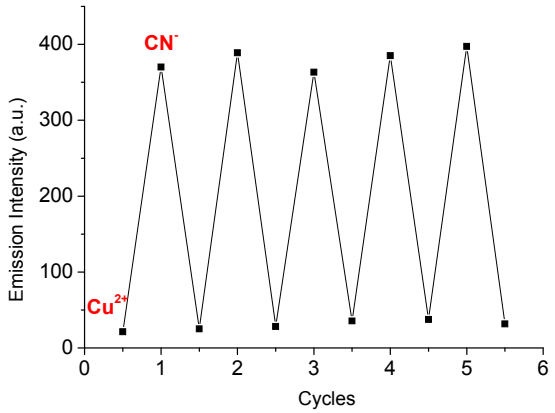

Fig. S39. Emission intensity changes of **2-Cu^{2+}** with alternately added CN^- and Cu^{2+}.

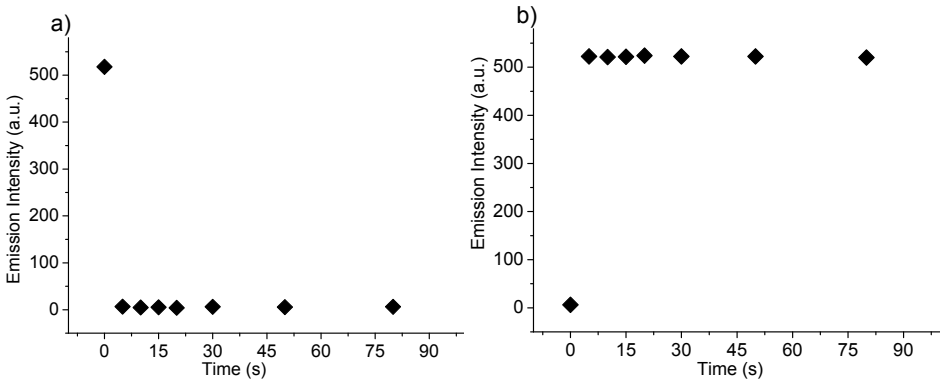

Fig. S40. Time course of the fluorescence response of **1** (10 μM) and **1-Cu^{2+}** (10 μM) in MeOH/H_2O, 4:1, v:v (λ_{ex} = 360 nm, λ_{em} = 438 nm): a) Compound **1** upon addition of 4 equiv. of Cu^{2+}; b) **1- Cu^{2+}** upon addition of 12 equiv. of CN^-.

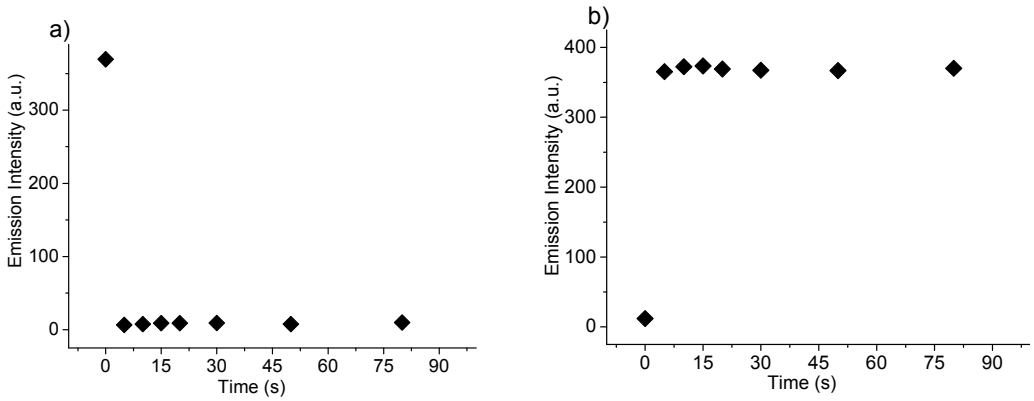

Fig. S41. Time course of the fluorescence response of **2** (10 μM) and **2-Cu^{2+}** (10 μM) in MeOH/H_2O, 4:1, v:v (λ_{ex} = 298 nm, λ_{em} = 437 nm): a) Compound **2** upon addition of 2 equiv. of Cu^{2+}; b) **2- Cu^{2+}** upon addition of 8 equiv. of CN^-.

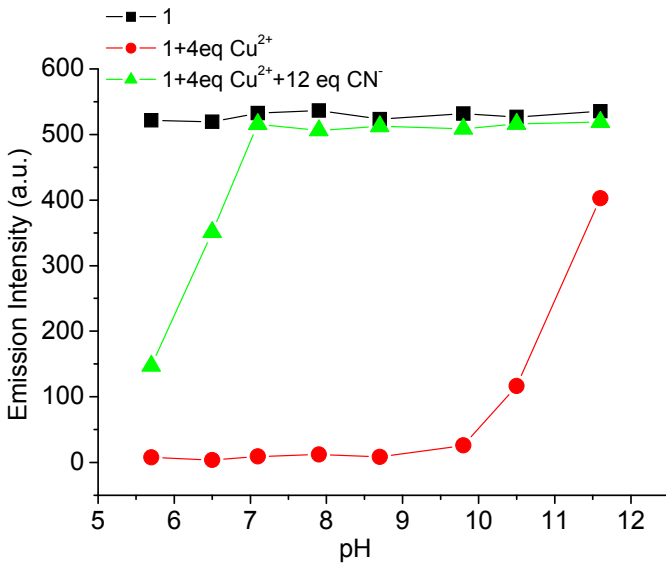

Fig. S42. Fluorescence emission of **1** (10 μM, black squares), **1**+4 eq Cu^{2+} (red circles), and **1**+4 eq Cu^{2+}+ 12 eq CN^- (green triangles) over the pH range 5-12.

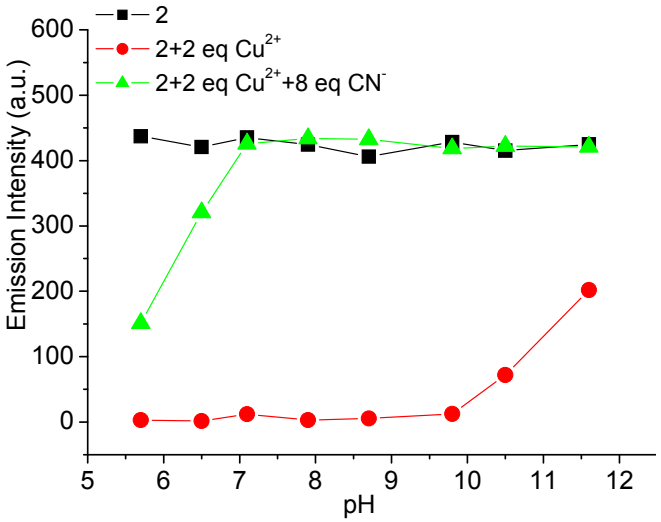

Fig. S43. Fluorescence emission of **2** (10 μM, black squares), **2**+2 eq Cu^{2+} (red circles), and **2**+2 eq Cu^{2+}+ 8 eq CN^{-} (green triangles) over the pH range 5-12.